CrystEngComm

Accepted Manuscript

ROYAL SOCIETY OF CHEMISTRY

www.rsc.org/crystengcomm

Cite this: DOI: 10.1039/c0xx00000x

www.rsc.org/xxxxxx

ARTICLE TYPE

Investigation of molecular arrangements and solid-state fluorescence properties on solvates and cocrystals of 1-acetyl-3-phenyl-5-(9-anthryl)-2-pyrazoline

Qi Feng,[a] Mingliang Wang,*[a] Chunxiang Xu,[b] Arshad Khan,[a] Xiaojuan Wu,[a] Jiao Lu,[a] Xiang Wei,[a]

Received (in XXX, XXX) Xth XXXXXXXXX 200X, Accepted Xth XXXXXXXXX 200X
DOI: 10.1039/b000000x

The title compound (APAP) was crystallized under different conditions to afford five types of crystals: the guest-free crystal (I), APAP·chloroform solvate (II), APAP·phenol cocrystal (III), APAP·2,2-bis(4-hydroxyphenyl)propane cocrystal (IV) and monohydrate (V). Single-crystal X-ray analysis revealed that a racemic chain motif is formed by the heterochiral APAP molecules in the guest-free crystal (I), in which anthracene fluorophores adopt face-to-face π-stacked arrangement. In contrast, by entrapment of different guest molecules, the homochiral chains are formed by one-handed enantiomers in crystals II-V, in which no effective π-overlap exists between anthracene fluorophores. The optical-physical properties of crystals I-IV and their structure-property relationship were investigated. Crystal I exhibits a broad emission band with only one peak centered at 458 nm. However, crystals II-IV exhibit the similar fluorescence spectra, in which the vibrational features are in good agreement with that of anthracene monomer emission and the λ_{em} are 430, 429 and 425 nm, respectively. As a control experiment we speculate, π-stacked arrangement of anthracene fluorophores should be responsible for larger red-shifted emission, lower emission quantum yield and longer lifetime. This strategy based on regulating the packing modes of anthracene fluorophores to tune the fluorescence properties and the investigation of structure-property relationship should be useful for the development of organic solid materials.

Introduction

Solid-state fluorescence properties of organic compounds have attracted much interest due to their direct and widespread applications in the fields of organic light-emitting diodes, organic photonics, and photoelectronic devices.[1-5] However, to design a solid-state luminescent organic material is a long standing problem owing to the fact that many organic flourophores that have strong fluorescence in solution lose this property in solid state.[6-8] An effective strategy to come up with a solution is by regulating the arrangements of fluorophores in solid state is core focus of the crystal engineers, because the arrangements strongly affect their solid-state fluorescence properties.[9-14] Therefore, for a given luminescent material, every different crystalline form (such as polymorphism, solvate and cocrystal) can be considered as a unique material with its own distinct properties.

Anthracene and pyrene derivatives have been studied extensively due to their excellent optical-physical properties,[15-18] such as their high fluorescence quantum yield and thermal stability. Unfortunately, these flat aromatic molecules in solid state are usually located in the immediate vicinity of each other (such as π-stacked arrangement), which result in their emission spectra shift to the longer wavelength with fluorescence efficiencies decreasing. [19] Thus, regulating the stacking modes of anthracene or pyrene fluorophores in solid state should be considered as an effective way for obtain the materials with desired properties and the investigation of relationship between the molecular arrangement and fluorescence properties is also important. [20-22]

In this study, we use 1-acetyl-3-phenyl-5-(9-anthryl)-2-pyrazoline (APAP) and its crystalline forms as a model, to analysis how anthracene fluorophores packing affects their optical-physical properties. Although the single crystal structure of APAP (crystal I) has been reported previously, [23] its optical-physical properties in solid state was not investigated. The fluorescence spectrum of APAP in *n*-hexane solvent (λ_{max} 412nm) is in good agreement with that of anthracene monomer, while in solid state, the spectrum shift to longer wavelength (λ_{max} 458nm) with disappearance of the vibrational features, which results in it greenish blue emission color. Crystal structure analysis revealed that anthracene fluorophores adopt face-to-face π-stacked arrangement. A speculation could be drawn that the red shift of fluorescence in solid state may be mainly caused by such π-stacked arrangement, since the similar structure-property relationship was also found in other systems.[20-21] In order to explore highly blue-emissive organic materials, we attempted to suppress the π-stacked arrangement by means of including other guest molecules in the lattice. Phenol was selected to co-crystallize with APAP, because it usually acts as a hydrogen bond donor and O-H···O hydrogen bonds could be expected to form

with acetyl group of APAP. Under different crystallization conditions, APAP·chloroforom solvate (II) and APAP·phenol cocrystal (III) were obtained. In addition, a small amount of colorless needle-like crystals appeared on the glass wall when we crystallize pure APAP in ethyl acetate solvent, which was not found previously and was identified as monohydrate (V) through single crystal X-ray diffraction analysis. However, this crystalline form has been got just once in spite of many trials. Although the anthracene fluorophores in crystals II, III and V are separated widely, the poor π-overlap between them were still found. Interestingly, crystals II and V exhibit the similar structures. The guests (chloroform or water molecules) connect not only with APAP but also with each other by themselves. Moreover, structure analysis indicated that the π-overlap between the neighboring anthracene fluorophores decreases with increasing the volume of the guest molecules (slight face-to-face and edge-to-face π-π interactions between anthracene fluorophores were found in crystals V and II, respectively). In view of these factors, 2,2-bis(4-hydroxyphenyl)propane (BPA) was used to co-crystallize with APAP. For one thing, BPA has a larger volume, which could be expected to prevent the π-stacked arrangement of anthracene fluorophores. For another, BPA could connect not only with APAP but also with themselves through hydrogen bonds, which were expected to construct the similar structure to crystals II and V. Although the structure of APAP·BPA cocrystal (IV) is different from that of crystals II and V, the anthracene fluorophores are separated more widely and adopt monomer arrangement. The thermal behaviors (in electronic supplementary information, Figures 1S and 2S, ESI†), FT-IR spectra (in electronic supplementary information, Figure 3S, ESI†), diffuse reflectance absorption spectra, solid-state fluorescence spectra, and fluorescence quantum yields and lifetimes of crystals I-IV were measured. The optical properties of these crystals as well as the anthracene arrangement modes in the structures were investigated. Since it was difficult to get an adequate amount of samples of V, only its single crystal data and fluorescence microscopy image could be obtained.

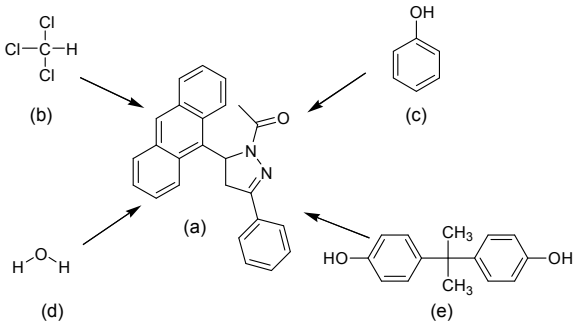

Scheme 1. Chemical structure of the fluorescent molecule (a, APAP) and the guest molecules (b, chloroform; c, phenol; d, H_2O; e, 2,2-bis(4-hydroxyphenyl)propane).

Experimental Section

Material Synthesis and Characterization

APAP was prepared by a reported method. [23] FT-IR (KBr, cm^{-1}): 3480, 3056, 2366, 1666, 1434, 1409, 1355, 1321, 1132, 930, 891, 789, 760, 739, 690, 640. ^{1}H NMR ($CDCl_3$, Figure 4S, ESI†): δ (ppm) 2.35 (s, 3H), 3.48-3.54 (dd, 1H), 3.88-3.94 (dd, 1H), 6.87-6.95 (dd, 1H), 7.31-7.34 (t, 1H), 7.36-7.39 (t, 1H), 7.45-7.48 (dd, 4H), 7.53-7.56 (t, 1H), 7.78-7.83 (m, 3H), 7.99-8.01 (d, 2H), 8.414 (s, 1H), 8.51-8.52 (d, 1H). ^{13}C NMR ($CDCl_3$, Figure 5S, ESI†): δ (ppm) 21.79, 41.61, 55.98, 122.83, 123.07, 124.49, 124.78, 126.04, 126.45, 126.60, 128.21, 128.40, 128.71, 129.29, 130.03, 130.27, 131.29, 131.37, 131.45, 131.83, 153.80, 169.46.

Crystal Growth

APAP (I) and its monohydrate (V). APAP was dissolved in ethyl acetate in a glass vial. Slow evaporation of the solvent at room temperature for 4-5 days, the yellow block crystals (I) in the rest mother liquor and a small amount of colorless needle-like crystals (V) on the glass wall were found simultaneously.

APAP·chloroform solvate (II). APAP was dissolved in chloroform/petroleum ether (v:v=1:1) or chloroform solvents in glass vials. Slow evaporation of the solvents at room temperature for 1-2 days yielded the colorless needle-like crystals.

APAP·phenol (III) and APAP·BPA (IV) cocrystals. APAP and phenol /BPA in an equimolar ratio were dissolved in ethyl acetate in a glass vials. Slow evaporation of the solvent at room temperature for 7-9 days yielded the colorless needle-like crystals (III) /colorless plate-like crystals (IV).

Measurements

Powder X-ray diffraction (PXRD) patterns for crystals I-IV were recorded using a 18KW advance X-ray diffractometer with Cu Kα radiation (λ=1.54056 Å). Single X-ray diffraction data for crystals II-V were collected on Nonius CAD4 diffractometer with Mo Kα radiation (λ= 0.71073 Å). The structures were solved with direct methods using the SHELXS-97 program [24] and refined anisotropically using full-matrix least-squares procedure. All non-hydrogen atoms were refined anisotropically and hydrogen atoms were inserted at their calculated positions and fixed at their positions.

^{1}H NMR and ^{13}C NMR spectra were recorded at 303 K on a Bruker Avance 300 MHz NMR spectrometer using $CDCl_3$ as solvent and TMS as internal standard. Infrared spectra were obtained with a Bruker Tensor 27 FT-IR spectrometer. Differential scanning calorimetry (DSC) and thermogravimetric analysis (TGA) patterns were recorded with a Mettler-Toledo TGA/DSC 1 Thermogravimetric Analyzer with the temperature scanned from 50 to 300 °C at 10 °C /min. UV-Vis absorption spectra were recorded on a Shimadzu UV-3600 spectrometer. Fluorescence spectra were obtained on a Horiba FluoroMax 4 spectrofluorometer. Fluorescence microscopy images were obtained on Olympus BX51 imaging system excited at 365 nm. Solid fluorescent quantum yields were performed using Quanta-φ accessory with excitation wavelength at 320 nm. Fluorescence lifetime measurements for the crystals were undertaken by the time-correlated single-photon counting technique (TCSPC) using a TemPro Fluorescence Lifetime System (Horiba Jobin Yvon) equipped with a NanoLed excitation source of 340 nm.

Result and discussion

Crystal structures

Single crystal X-ray diffraction analysis was performed for the

five crystals to determine their structures. All crystals II-V consist of 1:1 molar ratio between APAP and the guests (chloroform, phenol, BPA and water molecules). Only one independent APAP molecule is presented in the asymmetric unit (ASU, the ORTEP plots are presented in Figure 6S, ESI†) of the five crystals, which exhibits twisted structure with the dihedral angle between pyrazoline and anthracene rings of 76.94° (I), 88° (II), 75.12° (III), 86.43° (IV) and 71.93° (V). In addition, all the crystals are racemic due to the equimolar amounts of *R*- and *S*-APAP molecules in the unit cells. The crystallographic data are presented in Table 1. Intermolecular hydrogen bonds, π-π, C-H···π and C-Cl···π interactions in the crystals I-V are summarised in Tables 1S and 2S in electronic supplementary information.

Table 1. Numerical details of the solutions and refinements of crystals I-V.

crystal	I[23]	II	III	IV	V
Formula	$C_{25}H_{20}N_2O$	$C_{26}H_{21}Cl_3N_2O$	$C_{31}H_{26}N_2O_2$	$C_{40}H_{36}N_2O_3$	$C_{25}H_{22}N_2O_2$
Temperature/K	293	293	293	293	293
Crystal size/mm^3	0.30×0.24×0.20	0.20×0.10×0.10	0.20×0.10×0.10	0.30×0.20×0.10	0.20×0.10×0.10
morphology	block	needle	needle	plate	needle
Crystal system	Monoclinic	Monoclinic	Orthorhombic	Monoclinic	Monoclinic
Space group	$P2_1/n$	$P2_1/n$	$Pca2_1$	$P2_1/c$	$P2_1/n$
a/ Å	8.7102(17)	13.383(3)	22.826(5)	11.478(2)	10.258(2)
b/ Å	16.251(3)	9.766(2)	10.082(2)	15.142(3)	12.272(3)
c/ Å	13.309(3)	18.670(4)	10.677(2)	19.266(4)	16.034(3)
α/deg	90.00	90.00	90.00	90.00	90.00
β/deg	91.49(3)	100.97(3)	90.00	101.27(3)	105.53(3)
γ/deg	90.00	90.00	90.00	90.00	90.00
V/ Å^3	1883.2(7)	2395.5(8)	2457.1(8)	3283.9(11)	1944.8(7)
Z	4	4	4	4	4
ρ (calcd)/Mg m^{-3}	1.285	1.341	1.240	1.199	1.306
θ Range for data collection/°	3.03-25.60	1.73-25.50	1.78-25.35	1.72-25.39	2.12-25.43
F(000)	768	1000	968	1256	808
R_1, w R_2 ($I > 2\sigma(I)$)	0.0647, 0.1229	0.0741, 0.1330	0.0731, 0.1024	0.0659, 0.1466	0.0685, 0.1252
R_1, w R_2 (all data)	0.1272, 0.1423	0.1820, 0.1697	0.1722, 0.1278	0.1580, 0.1906	0.1601, 0.1519
Goodness-of-fit	1.040	1.006	1.000	1.003	1.002
CCDC	968929	968812	968814	968811	968813

Crystal I has a monoclinic system and space group $P2_1/n$. In the structure, the heterochiral molecules associate through weak C-H···O hydrogen bonds in a molar ratio of 1:1 along the *a* axis to form a racemic chain motif (Figure 1a), in which the two neighboring anthracene rings form a dimer and adopt face-to-face π-stacked arrangement (Figure 1b) with a centroid-centroid distance and a interplanar separation of 5.414 and 3.232 Å (the lateral displacement is 4.34 Å). The chains are stacked in a parallel fashion to form its three-dimensional (3D) structure (Figure 1c).

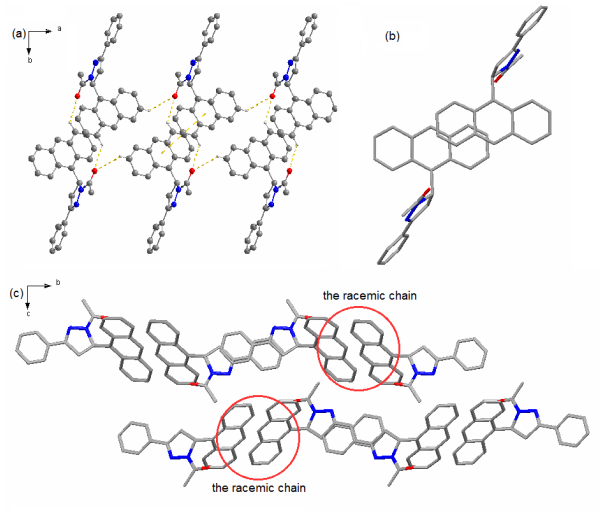

Figure 1. Structure of crystal I. (a) Racemic chain *via* hydrogen bond and π-stacking interactions between the neighboring anthracene rings. (b) Top view of adjacent APAP molecules along the plane of anthracene stacking. (c) 3D packing diagram of crystal I projected in *bc* plane. The dotted lines show hydrogen bonds and π-π interaction, respectively. Hydrogen atoms not participating in the interactions have been omitted for clarity.

Crystal II has a monoclinic system and space group $P2_1/n$. In the structure, the one-handed enantiomers associate along the *b* axis through C-H···π interactions to construct a homochiral helical chain motif. As shown in Figure 2a, the nearest C-H···*c* distance (the centre of one six-membered ring of the anthracene) between the neighboring anthracene rings in the homochiral chain is 3.04 Å, suggesting that the anthracene rings are separated widely and poor π-overlap exists between them. The chloroform molecules are linked with APAP by hydrogen bond and weak C-Cl···π interactions (Figure 2a) and reside in the channels along the *b* axis (Figure 2b). Moreover, the neighboring chloroform molecules associate through C-Cl···Cl-C interaction (C26-Cl1···Cl1-C26, the distance between two chloroform molecules is 3.215(4) Å, θ1=θ2=146.9(3) °, θ is C-Cl···Cl angle), which play a bridging role in associating two neighboring homochiral helical chains with opposite chirality.

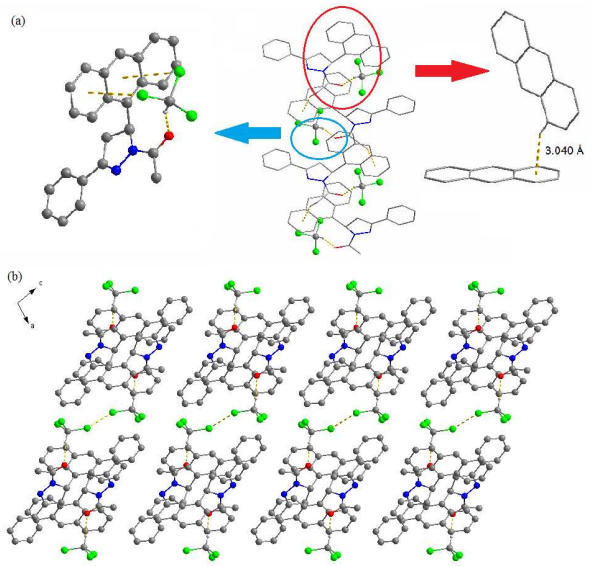

Figure 2. Structure of crystal II. (a) The homochiral helical chain motif, inermolecular interactions between APAP and chloroform and C-H···π interaction between the two neighboring anthracene rings in the homochiral chain. (b) 3D packing diagram of crystal II (projected in *ac* plane). The dotted lines show hydrogen bonds, C-Cl···π and C-H···π interactions, respectively. Hydrogen atoms not participating in the interactions have been omitted for clarity.

Crystal III has an orthorhombic system and space group $Pca2_1$. APAP is linked with phenol molecule through O-H···O hydrogen bond. In the structure, the one-handed enantiomers associate along the *c* axis through hydrogen bond, C-H···π and π-π interactions to construct a homochiral helical chain motif (Figure 3a). C-H···π interaction between the anthracene rings was also found in the homochiral chain with the nearest C-H···*c* distance of 2.97 Å, suggesting that the π-overlap between the anthracene rings is also very poor. The homochiral chains with opposite chirality are stacked alternately along the *a* axis and are stacked in a parallel fashion along the *b* axis to construct the 3D structure (Figure 3b).

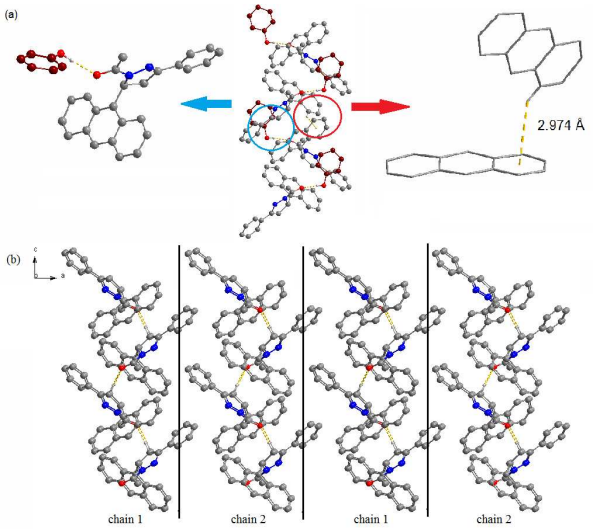

Figure 3. Structure of crystal III. (a) The homochiral helical chain motif, inermolecular interactions between APAP and phenol and C-H···π interaction between the two neighboring anthracene rings in the homochiral chain. (b) 3D packing diagram of crystal III (projected in *ac* plane, chains 1 and 2 are the homochiral chains with opposite chirality). The dotted lines show hydrogen bonds and C-H···π interactions, respectively. Gray and brown colored molecules are APAP and phenol molecules respectively. Hydrogen atoms not participating in the interactions have been omitted for clarity.

Crystal IV has a monoclinic system and space group $P2_1/c$. The dihedral angle between the two benzene rings of BPA molecule is 80.14°. As shown in Figure 4a, BPA molecules are linked with each other through O-H···O hydrogen bond along *a* axis to form 1D BPA-chain structure, which are also linked with the one-handed enantiomers of APAP in 1:1 molar ratio by hydrogen bonds and C-H···π interactions to give a homochiral chain motif. In addition, BPA molecules play a bridging role in associating two neighboring homochiral chains with opposite chirality through C-H···O hydrogen bond to give a columnar structure (Figure 4b). Such columns associate to construct the overall racemic 3D structure. In this structure, the anthracene rings are widely separated with the closest centroid distance of 6.784 Å, suggesting no π-π interactions exists between them.

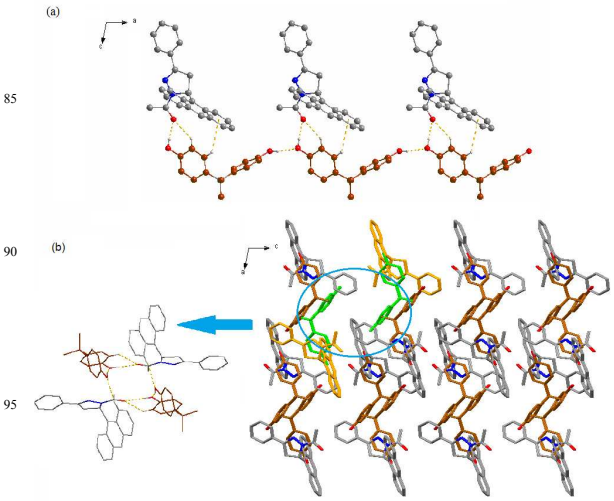

Figure 4. Structure of crystal IV. (a) 1D chain structure and interactions between BPA and APAP molecules and two neighboring BPA molecules. (b) The racemic column constructed by two homochiral chains with opposite chirality and 3D packing diagram of crystal IV (projected in *ac* plane). The dotted lines show hydrogen bonds and C-H···π interactions, respectively. Gray and brown colored molecules are APAP and BPA molecules respectively. Hydrogen atoms not participating in the interactions have been omitted for clarity.

Crystal V has a monoclinic system and space group $P2_1/n$. Interestingly, this structure is similar to crystal II. The one-handed enantiomers associate along the *b* axis through C-H···π interactions to construct a homochiral helical chain motif (Figure 5a). The water molecules are linked with APAP by hydrogen bond and reside in the channels along the *b* axis. The two neighboring water molecules connect with each other through hydrogen bond interaction and also play a bridging role in associating the two neighboring homochiral chains with opposite

chirality (Figure 5b). However, due to the small volume of water molecules, the two neighboring homochiral chains are close to each other and a small degree of π-overlap between adjacent anthracene rings was found. The centroid-centroid distance and interplanar separation are 7.191 and 3.512 Å, respectively (the lateral displacement is 6.27 Å).

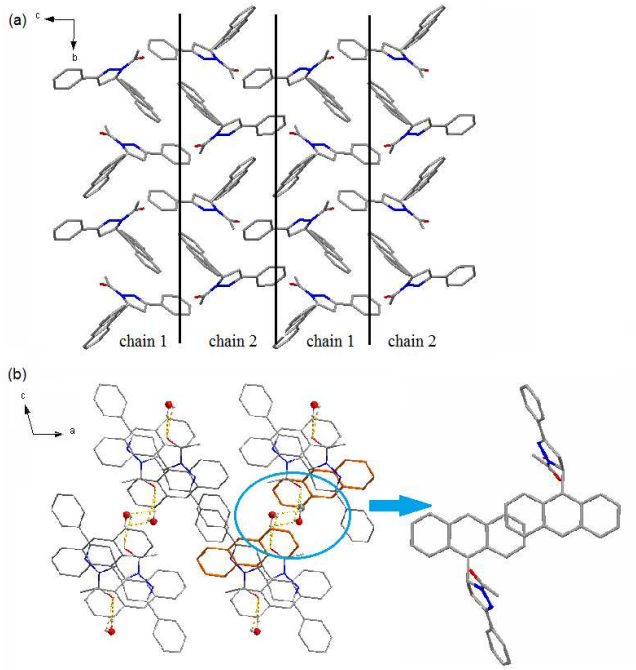

Figure 5. Structure of crystal V. (a) Homochiral helical chains (chains 1 and 2 are the homochiral chains with opposite chirality). (b) 3D packing diagram of crystal V projected in *ac* plane and the top view of adjacent APAP molecules along the plane of anthracene stacking. The dotted lines show hydrogen bonds. Hydrogen atoms not participating in the interactions have been omitted for clarity.

Powder X-ray diffraction (PXRD) patterns

Before investigation of the optical properties, it should be confirmed that the samples possess a unique crystalline phase. The PXRD of I-IV was performed and their patterns (Figure 6a) are in agreement with that simulated from their single crystal data (Figure 6b), suggesting the samples can be used for other measurements later.

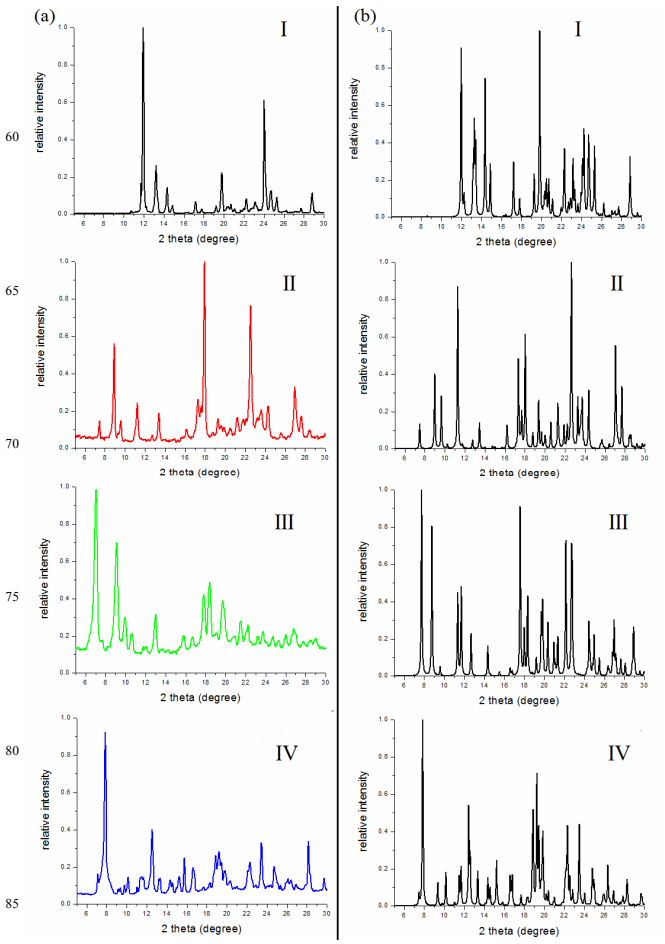

Figure 6. PXRD patterns of crystals I-IV: (a) experimental PXRD patterns and (b) simulated patterns.

Optical-physical properties

Diffuse reflectance absorption and fluorescence emission spectra (Figures 7 and 8) were exploited to investigate the optical-physical properties of crystals I-IV. The absorption spectra of APAP in solvents are structured (Figure 7S, ESI†), with band maxima only slightly red-shifted compared to that of anthracene. In solid state, crystals II-IV show the similar absorption bands with three peaks located at 350-450 nm arising from anthracene, which are similar to the spectra measured in solvents. However, crystal I exhibits a broader band with a red shift of about 10 nm relative to that of crystals II-IV, in which the characteristic vibrational fine structures are also less clear. This difference should be attributed to their different arrangements of anthracene fluorophores, the aggregation of anthracene fluorophore (face-to-face π-stacked geometries) in crystal I is responsible for its broader and red-shifted absorption band. [25]

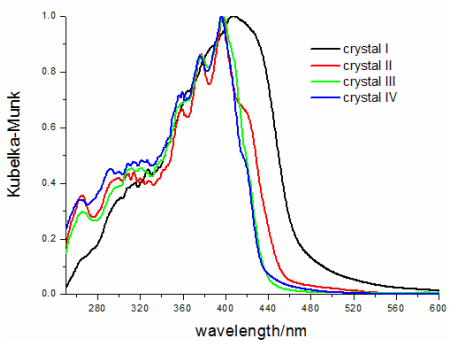

Figure 7. Absorption spectra of crystals I-IV.

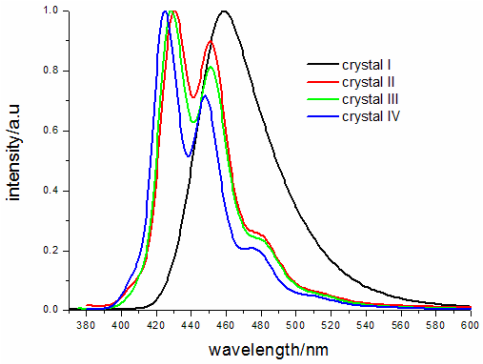

Figure 8. Fluorescence spectra of crystals I-IV (λ_{ex}=365nm).

The fluorescence spectrum of APAP in *n*-hexane solvent (Figure 8S, ESI†) mainly exhibits three vibrational peaks at 391, 412 and 437 nm, corresponding to the anthracene monomer emission. In solid state, the emission spectra of crystals II-IV are similar to each other. They mainly exhibit three peaks located at 410-490 nm, which are the mirror images of their absorption spectra and are similar to its fluorescence spectra measured in solvents. However, crystal I shows a structureless emission profile, which exhibits a broad emission band with only one peak centered at 458 nm. According to these crystal structures, all APAP molecules exhibit twisted structures in solid state with the large dihedral angles between pyrazoline ring and anthracene ring (the range from 75.12 to 86.43°), which suggests that the very small degree of π-conjugation between the two rings and the molecular conformation of APAPs have little influence on their fluorescence properties. Thus, these results clearly demonstrate that the optical-physical properties of the crystals are anthracene fluorophores-arrangement-dependent, while the interactions between the host and guest molecules are the reason for different arrangements of anthracene fluorophores in these crystals, although they don't have strong interaction with anthracene. Based on the preceding crystal structure analysis, because anthracene fluorophores are situated apart from each other in crystals II-IV (although C-H···π interaction between anthracene fluorophores was found in crystals II and III, the nearest C-H···*c* distance indicates that no effective π-overlap exists between them), their emission bands are similar to each other and the vibrational features are in good agreement with anthracene monomer emission. Moreover, in these three crystals, crystal IV exhibits the shortest λ_{em}, which may be relevant to the monomer arrangement of anthracene fluorophores in the structure. In general, the π-π stacking geometry has an interplanar separation of 3.4-3.6 Å and lateral displacement of 1.6-1.8 Å.[26-28] However, anthracene florophores in crystal I are arranged with a longer lateral displacement of 4.34 Å and a shorter interplanar separation of 3.23 Å. Such anthracene dimer was relatively few in the previous reports and the arrangement is similar to the salt of anthracene-1,5-disulfonic acid and *n*-propylamine (nPrA, the lateral displacement and interplanar separation between anthracene rings are 4.72 and 3.30 Å, respectively), which results in a red-shift of the solid-state spectrum (λ_{max} 452 nm), suggesting that the effective π-overlap still exists between the anthracene fluorophores, although the lateral displacement is longer than that of the usual π-stacked geometry. [29] Therefore, the red-shifted and structureless emission spectrum of crystal I should be attributed to the slipped face-to-face π-stacking of anthracene fluorophores in the structure. Irradiating the crystals with UV light reveals that they show different fluorescence colors from greenish blue to blue (Figure 9). Moreover, corresponding to the blue emission color of crystal V and its crystal structure (the lateral displacement between the anthracene fluorophores is 6.27 Å), a conclusion can be drawn that the effective π-overlap of anthracene fluorophores probably no longer exists in the largely separated geometry and its emission band should be similar to that of crystals II-IV.

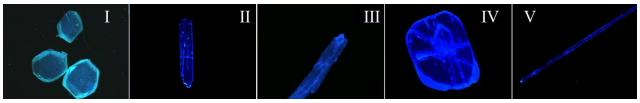

Figure 9. Fluorescence microscopy images of crystals I-V (λ_{ex}=365nm).

Emission quantum yields (Φ_F) and fluorescence lifetimes (τ_F) were measured to obtain further insight into their optical-physical properties. For our system, the Φ_F values of blue-emissive crystals are slight higher than that of greenish blue-emissive crystal, as summarized in Table 2. The difference in the solid-state Φ_F values should be attributed to the different stacking arrangements of anthracene fluorophores. The π-stacked geometries of anthracene fluorophores are responsible for the lower fluorescence efficiencies in solid-state, and suppression of such π-π interaction should be an effective way for achieving bright blue-emissive materials. In contrast, the fluorescence decays (Figure 10S, ESI†) show that crystal I exhibits longer fluorescence lifetime than others. This difference may be relative to the immobilization of anthracene fluorophores in the crystal. The intermolecular interactions originated from the π-overlap of two adjacent anthracene fluorophores in crystal I may suppress the nonradiative relaxation process, which leads to its longer lifetime.

Table 2. Optical-physical properties data of crystals I-IV.

crystals	λ_{ab}(nm)[a]	λ_{ex}(nm)[b]	λ_{em}(nm)[c]	Φ_F[d]	τ_F (ns) [e]
I	407	363	458	0.054	12.84
II	397	364	430	0.077	10.72
III	398	365	429	0.084	6.57
IV	396	364	425	0.069	5.75

[a] maximum wavelengths of diffuse reflectance absorption spectra; [b] maximum wavelengths of fluorescence excitation spectra monitored at

their respective maximum emission peaks (Figure 9S, ESI†); [c] wavelengths of fluorescence emission spectra excited at 365nm for crystals I-IV; [d] fluorescent quantum yields excited at 320nm; [e] fluorescence lifetimes excited at 340 nm.

Conclusions

In summary, we demonstrated that regulating the packing modes of anthracene fluorophores by means of entrapment of different guest molecules result in different fluorescent colors. Crystal structures revealed that anthracene fluorophores adopt face-to-face π-stacked arrangement, while in crystals II-V, anthracene fluorophores are separated widely and no effective π-overlap exists between them. These different stacking modes modulated their fluorescent colors from greenish-blue to blue. The investigation of structure-property relationship revealed that the suppression of π-stacked geometries of anthracene fluorophores is crucial for achieving highly blue-emissive materials. This strategy based on the host-guest structure for fluorescence modulation and the investigation of structure-property relationship are useful for designing various new types of organic solid materials.

Acknowledgment

This project gets the supports of the National Basic Research Program of China (2011CB302004).

Notes and references

[a] *School of Chemistry and Chemical Engineering, Southeast University, Nanjing 211189, P. R. China.Tel.: +86 2585092237. E-mail: wangmlchem@seu.edu.cn*
[b] *State Key Laboratory of Bioelectronics, Southeast University, Nanjing 210096, P. R. China. E-mail: xcxseu@seu.edu.cn*

† Electronic Supplementary Information (ESI) available: [Thermal and FT-IR studies, ^{1}H and ^{13}C NMR spectra of APAP, ORTEP plots of five crystals, parameters of intermolecular hydrogen bonds, π-π, C-H···π and C-Cl···π interactions in the crystals I-V, absorption and emission spectra of APAP in various solvents, exiciation spectra of crystals I-IV and fluorescence decay curves for crystals I-IV, X-ray crystallographic imformation files (CIF) for crystals II-V] See DOI: 10.1039/b000000x/

1 A. W. Czarnik, *Acc. Chem. Res.*, 1994, **27**, 302–308.
2 F. Gao, Q. Liao, Z. Xu, Y. Yue, Q. Wang, H. Zhang and H. Fu, *Angew. Chem., Int. Ed.*, 2010, **49**, 732–735
3 D. P. Yan, J. Lu, J. Ma, M. Wei, D. G. Evans and X. Duan, *Angew. Chem., Int. Ed.*, 2011, **50**, 720–723.
4 C. A. Strassert, C. H. Chien, M. D. G. Lopez, D. Kourkoulos, D. Hertel, K. Meerholz and L. D. Cola, *Angew. Chem., Int. Ed.*, 2011, **50**, 946−950.
5 J. Schmidtke, W. Stille, H. Finkelmann and S. T. Kim, *Adv. Mater.*, 2002, **14**, 746−749.
6 H. Langhals, O. Krotz, K. Polborn and P. Mayer, *Angew. Chem., Int. Ed.*, 2005, **44**, 2427−2428.
7 A. Dreuw, J. Plotner, L. Lorenz, J. Wachtveitl, J. E. Djanhan, J. Bruning, T. Metz, M. Bolte and M. U. Schmidt, *Angew. Chem., Int. Ed.*, 2005, **44**, 7783−7786.
8 J. N. Moorthy, P. Venkatakrishnan, P. Natarajan, D. F. Huang and T. J. Chow, *J. Am. Chem. Soc.*, 2008, **130**, 17320−17333.
9 Y. Mizobe, N. Tohnai, M. Miyata and Y. Hasegawa, *Chem. Commun*., 2005, 1839−1841.
10 G. Q. Zhang, J. W. Lu, M. Sabat and C. L. Fraser, *J. Am. Chem. Soc.*, 2010, **132**, 2160−2162.
11 D. P. Yan and D. G. Evans, Mater. Horiz., 2014, **1**, 46–47.
12 D. P. Yan, W. Jones, G. L. Fan, M. Wei and D. G. Evans, J. Mater. Chem. C, 2013, **1**, 4138–4145.
13 R. Davis, N. P. Rath and S. Das, *Chem. Commun*., 2004, 74−75.
14 I. Hisaki, E. Kometani, H. Shigemitsu, A. Saeki, S. Seki, N. Tohnai and M. Miyata, *Cryst. Growth Des*., 2011, **11**, 5488−5497.
15 C. H. Wu, C. H. Chien, F. M. Hsu, P. I. Shih and C. F. Shu, *J. Mater. Chem.*, 2009, **19**, 1464−1470.
16 Y. Kan, L. Wang, L. Duan, Y. Hu, G. Wu and Y. Qiu, *Appl. Phys. Lett.*, 2004, 1513−1515.
17 K. Danel, T. H. Huang, J. T. Lin, Y. T. Tao and C. H. Chuen, *Chem. Mater.*, 2002, **14**, 3860−3865..
18 H. M. Kim, Y. O. Lee, C. S. Lim, J. S. Kim and B. R. Cho, *J. Org. Chem*., 2008, **73**, 5127−5130.
19 Y. N. Hong, J. W. Y. Lam and B. Z. Tang, *Chem. Soc. Rev*., 2011, **40**, 5361−5388.
20 Q. Feng, M. L. Wang, B. L. Dong, C. X. Xu, J. Zhao and H. J. Zhang, *CrystEngComm*., 2013,**15**, 3623−3629.
21 B. L. Dong, M. L. Wang, C. X. Xu, Q. Feng and Y. Wang, *Cryst. Growth Des*., 2012, **12** , 5986−5993.
22 Z. L. Zhang, Y. Zhang, D. D. Yao, H. Bi, I. Javed, Y. Fan, H. Y. Zhang and Y. Wang, *Cryst. Growth Des.*, 2009, **9** , 5069−5076.
23 M. L. Wang, B. L. Dong and Y. H. Li, *Acta Crystallogr. Sect. E*, 2011, E**67**, o94.
24 G. M. Sheldrick, SHELXS97: Programs for Crystal Structure Analysis, University of Göttingen, Germany.
25 F. Wilkinson, D. R. Worrall and S. L. Williams, *J. Phys. Chem.*, 1995, **99**, 6689−6636.
26 L. M. Salonen, M. Ellermann and F. Diederich, *Angew. Chem., Int. Ed.*, 2011, **50**, 4808−4842.
27 E. A. Meyer, R. K. Castellano and F. Diederich, *Angew. Chem., Int. Ed.*, 2003, **42**, 1210−1250.
28 M. D. Curtis, J. Cao and J. W. Kampf, *J. Am. Chem. Soc.*, 2004, **126**, 4318−4328.
29 T. Hinoue, Y. Shigenoi, M. Sugino, Y. Mizobe, I. Hisaki, M. Miyata and N. Tohnai, *Chem. Eur. J.*, 2012, **18**, 4634–4643.